






Predicting the Structure of the Solar Corona and Inner Heliosphere during *Parker Solar Probe's* First Perihelion Pass

Pete Riley , Cooper Downs , Jon A. Linker , Zoran Mikic , Roberto Lionello , and Ronald M. Caplan 

Predictive Science Inc. 9990 Mesa Rim Road, Suite 170, San Diego, CA 92121, USA; pete@predsci.com

Received 2019 February 25; revised 2019 March 11; accepted 2019 March 12; published 2019 March 28

Abstract

NASA's *Parker Solar Probe* (*PSP*) spacecraft reached its first perihelion of 35.7 solar radii on 2018 November 5. To aid in mission planning, and in anticipation of the unprecedented measurements to be returned, in late October, we developed a three-dimensional magnetohydrodynamic (MHD) solution for the solar corona and inner heliosphere, driven by the then available observations of the Sun's photospheric magnetic field. Our model incorporates a wave-turbulence-driven model to heat the corona. Here, we present our predictions for the structure of the solar corona and the likely in situ measurements that *PSP* will be returning over the next few months. We infer that, in the days prior to first encounter, *PSP* was immersed in wind emanating from a well-established, positive-polarity northern polar coronal hole. During the encounter, however, field lines from the spacecraft mapped to a negative-polarity equatorial coronal hole, within which it remained for the entire encounter, before becoming magnetically connected to a positive-polarity equatorial coronal hole. When the *PSP* data become available, these model results can be used to assist in their calibration and interpretation, and, additionally, provide a global context for interpreting the localized in situ measurements. In particular, we can identify what types of solar wind *PSP* encountered, what the underlying magnetic structure was, and how complexities in the orbital trajectory can be interpreted within a global, inertial frame. Ultimately, the measurements returned by *PSP* can be used to constrain current theories for heating the solar corona and accelerating the solar wind.

Key words: magnetohydrodynamics (MHD) – solar wind – Sun: corona – Sun: heliosphere – Sun: magnetic fields – waves

1. Introduction

Parker Solar Probe (*PSP*) was launched on 2018 August 12. Through the use of seven gravity assists from Venus, it will, over a total of 24 orbits, reach a final heliocentric distance of 9.86 solar radii (R_{\odot}) (Fox et al. 2016). At closest approach it will be traveling at speeds approaching 200 km s^{-1} , comparable to, or greater than the expected local speed of the solar wind at this distance. The primary scientific goals of the mission are to: (1) better understand what heats the solar corona and accelerates the solar wind; (2) determine the underlying structure and dynamics of the coronal magnetic field; and (3) better identify the mechanisms that accelerate and transport energetic particles in the corona (Fox et al. 2016).

PSP is carrying four instrument packages. FIELDS (Electromagnetic Fields Investigation) consists of two flux-gate magnetometers, a search-coil magnetometer, and five plasma voltage sensors (Bale et al. 2016). It measures electric and magnetic fields, as well as radio waves, Poynting flux, plasma density, and electron temperature. ISoIS (Integrated Science Investigation of the Sun) consists of two separate instruments: EPI-Hi and EPI-Lo, which measure energetic electrons, protons, and heavy ions (McComas et al. 2016). Solar Wind Electrons Alphas and Protons (SWEAP) is composed of three instruments: two electrostatic analyzers and one Faraday cup, from which estimates of velocity, density, and temperature of electrons, protons, and alpha particles can be made (Kasper et al. 2016). Finally, Wide-field Imager for Solar Probe (WISPR) comprises of two optical telescopes that provide coronagraph-like images of the corona and heliosphere (Vourlidas et al. 2016).

Global models of the solar corona and inner heliosphere are important tools for complementing any spacecraft mission

(e.g., Pizzo & Gosling 1994; Linker et al. 1999; Riley et al. 2001; Aschwanden et al. 2008; Török et al. 2018). However, this is particularly true for *PSP*, given its unique trajectory, narrow temporal windows for each encounter, and limited instrumentation. Most recently, we have developed a global, time-dependent magnetohydrodynamic (MHD) model, MHD Algorithm outside a Sphere (MAS), which includes the effects of waves and turbulence to heat the corona, and the WKB approximation for wave pressures to accelerate the solar wind (Mikic et al. 2018). Thus, it is particularly suitable for interpreting *PSP* measurements.

In this report, we describe the results of MHD model solutions aimed at predicting what *PSP* will have observed around first encounter (2018 October 31 to November 11) during which time the spacecraft remains within 0.25 au of the Sun. Although the measurements have already been made by the spacecraft, these simulations were completed prior to first encounter (2018 October 30), and their interpretation is currently being made before the data have been publicly released. In this sense, it represents an informal prediction of the “future” state of the corona. In Section 2, we first provide an analytical summary of *PSP's* unique trajectory before reviewing the MHD solutions. We next present a global MHD model, and use the results to magnetically map *PSP's* trajectory back to the solar surface, predicting the likely origin of the solar wind plasma and magnetic field that *PSP* was immersed in during the first encounter. We then compare these model solutions with a Potential Field Source Surface (PFSS) model highlighting the differences between them. Finally, we fly the spacecraft through our heliospheric solutions producing a prediction of the plasma and magnetic field measurements that the FIELDS and SWEAP instruments will have made. We

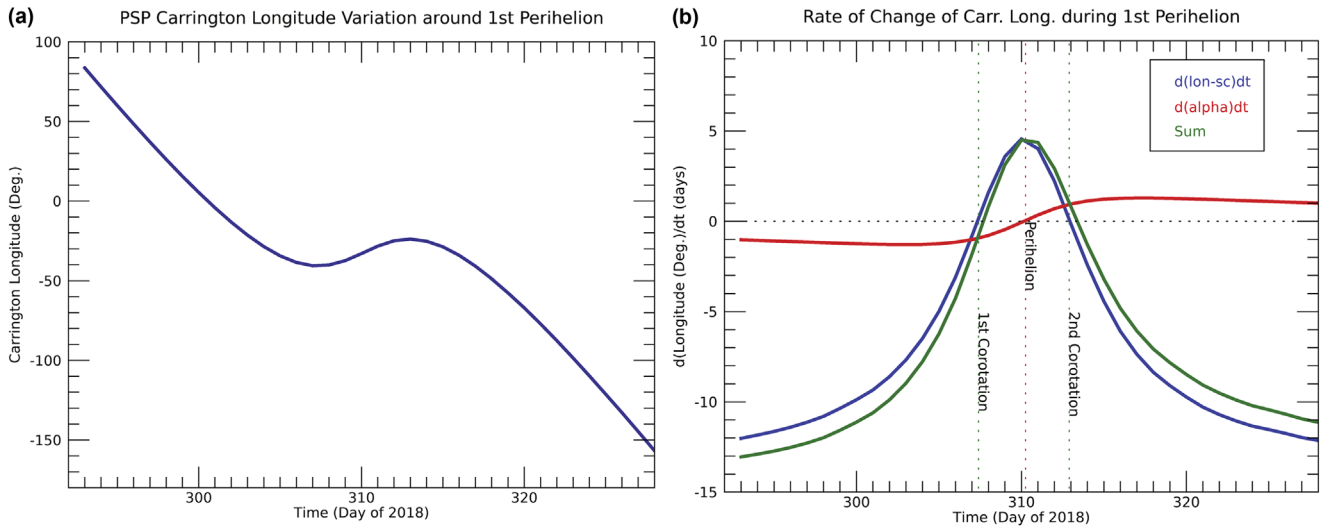


Figure 1. (a) Variation of *PSP*'s Carrington longitude position as a function of time during first encounter. (b) Variation of the time rate of change of *PSP*'s Carrington longitude (blue), foot-print location based on its radial motion (red), and the sum of these two effects (green) as a function of time during first encounter.

conclude by discussing the implications of this study and anticipating how future encounters, complemented by measurements from Solar Orbiter, can provide additional constraints on the models, and lead to a better understanding of the physical processes at work.

2. Analytic Analysis

Before discussing the MHD model, it is worth briefly considering some unique aspects of the *PSP* trajectory. Unlike many previous spacecraft, such as *Wind*, *ACE*, *STEREO A* and *B*, which traveled at an approximately constant rate in azimuth, because of its evolving eccentric orbit, *PSP* sweeps ever faster azimuthally as it approaches perihelion. This has implications for which magnetic field lines intercept the spacecraft, and, by extension, changes the inferred source region of the plasma being measured. Relative to Carrington coordinates, which is a fixed system rotating at a rate of 25.38 days, the spacecraft moves backward in Carrington longitude until approximately the beginning of first encounter, when it corotates with the Sun. It then travels faster than the Sun's surface (at least that part that is traveling with an angular velocity of $2\pi/25.38$ rads/day) briefly, before reaching a point of corotation again, and finally drifting further back in Carrington longitude (Figure 1(a)). Between these two points of corotation lies perihelion, at $35.7 R_S$.

In addition to the direct effect of crossing solar meridians, an indirect effect occurs because of *PSP*'s radial motion. As described by Parker (1958), magnetic field lines convected out by the super-Alfvénic solar wind become increasingly wound up as the Sun rotates underneath them. This Archimedean pattern results in field lines of approximately 45° at 1 au for wind traveling at $\sim 450 \text{ km s}^{-1}$. As the spacecraft accelerates into perihelion, it moves ever faster toward the Sun, which has the effect of causing it to sample these Archimedean field lines that connect progressively further to the east. This can be written as:

$$\Delta\alpha = \frac{\Delta R(\text{km})}{v(\text{km s}^{-1})} \frac{360^\circ}{25.38 \times 86,400 \text{ s}}, \quad (1)$$

where ΔR is the change in heliocentric distance, and v is the speed of the solar wind. This and the preceding effect are summarized in Figure 1(b), which shows the time rate of change in the foot-point location of field lines connected to *PSP* due to its azimuthal motion (blue) and the radial motion (red). The former dominates, but, when combined (green), it has the overall effect of making the connectivity asymmetric, due to the fact that the radial motion is not symmetric around perihelion. Overall then, both first and second corotation are later in time with respect to perihelion, and, thus, the outward portion of the encounter lasts approximately one day longer than the inward portion, with respect to the points of corotation.

3. Modeling Approach

In this study we used the MAS code, which solves the set of resistive MHD equations in spherical coordinates on a nonuniform mesh. The details of the model have been described elsewhere (e.g., Mikić & Linker 1994; Lionello et al. 2001; Riley et al. 2001, 2012; Caplan et al. 2017; Mikić et al. 2018). Here, we restrict our description to several relevant points. First, the model is driven by the observed photospheric magnetic field. We used HMI magnetograph observations from the SDO spacecraft to construct a boundary condition for the radial magnetic field at $1 R_S$ as a function of latitude and longitude. In particular, given the requirement of making the prediction prior to the start of first encounter, we built up a map based on observations during Carrington rotation (CR) 2208 and 2209. As a practical limitation, because *PSP* was effectively located at quadrature to Earth, during perihelion, this meant that the data lying under the spacecraft at the point of closest approach was approximately one week old (because it was observed from Earth, and rotated westward to build up the map). Additionally, due to inaccuracies stemming from projection effects, we applied a pole-fitting procedure to reconstruct the poorly observed polar regions, as described by Mikić et al. (2018). Second, the model is run in two stages: first the region from 1 to $30 R_S$ is modeled, followed by the region from $30 R_S$ to 1 au, being driven directly by the results of the coronal calculation. Computationally, this approach is

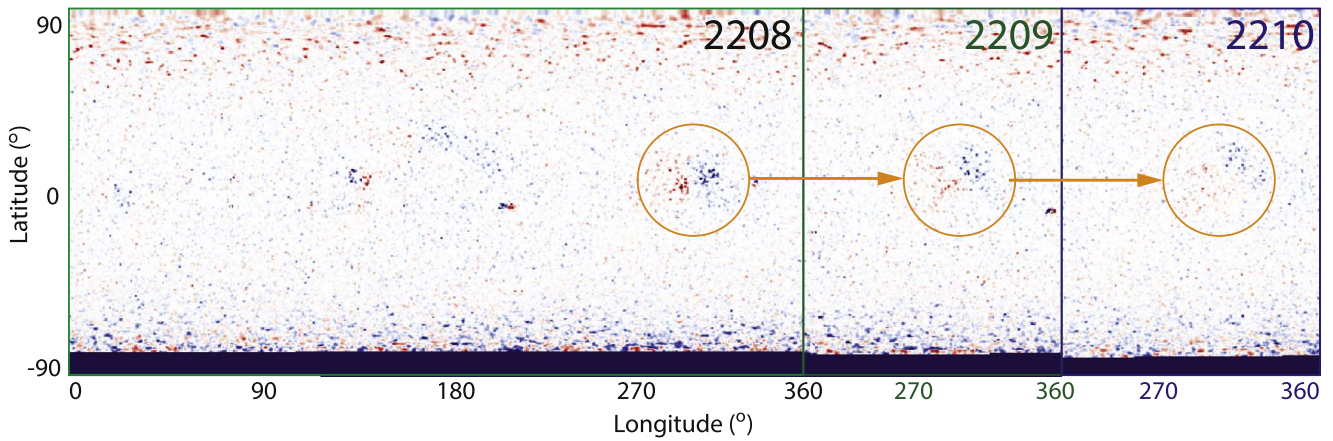


Figure 2. Synoptic maps (Carrington longitude vs. heliographic latitude) of the photospheric magnetic field for CR 2208, and parts of 2209 and 2210, showing the evolution of the active region at $\sim 330^\circ$ longitude.

much more efficient, and, by overlapping the region between the simulations, we verified that the transition is seamless (Lionello et al. 2013). Third, as noted above, this version of the model implements a Wave-Turbulence-Driven (WTD) approach for self-consistently heating the corona and invokes the WKB approximation for wave pressures, providing the necessary acceleration of the solar wind (Mikic et al. 2018). The physical motivation for this heating model is that outward and reflecting Alfvén waves interact with one another, resulting in their dissipation, and heating of the corona (e.g., Zank et al. 1996; Verdini & Velli 2007). We have found that this approach can account for both the acceleration of solar wind along open field lines, as well as the heating of plasma entrained within closed-field regions (Lionello et al. 2014; Downs et al. 2016).

4. Results

The boundary conditions used to drive the WTD coronal model are summarized in Figure 2. As described by Mikic et al. (2018), we multiplied the HMI-derived synoptic maps by a factor of 1.4 to account for the difference in magnetic field strengths measured by the HMI instrument as compared to its predecessor, MDI on board the *Solar and Heliospheric Observatory*. As noted above, we initiated our production run one week prior to the beginning of first encounter, which required that we combine maps from CR 2208 and 2209. Since *PSP* was at quadrature relative to the Earth at Perihelion it is not clear whether more timely data would have improved the accuracy of the solution. Retrospectively, however, it was useful to compare data near Carrington longitude 330° for CRs 2208, 2209, and 2210 (Figure 2). During these rotations the active region lying under the spacecraft evolved significantly, becoming progressively weaker. This allows us, at least in a heuristic sense, to estimate likely uncertainties from a region that was neither well observed nor stationary in time.

The WTD-driven model was run using the aforementioned synoptic map out to $30 R_S$. Then the output from this run was used to directly drive a second simulation from $29 R_S$ to 1 au. Once complete, these data were interpolated onto a common grid and the orbital trajectory of *PSP* was flown through the results. For each day, over a week prior to and following the encounter field lines at the spacecraft’s location were traced back to the Sun. These are shown in Figures 3(a)–(c). Each field line is drawn (in an arbitrary, but consistent color) and a selection of them is stamped with the relevant date for that field

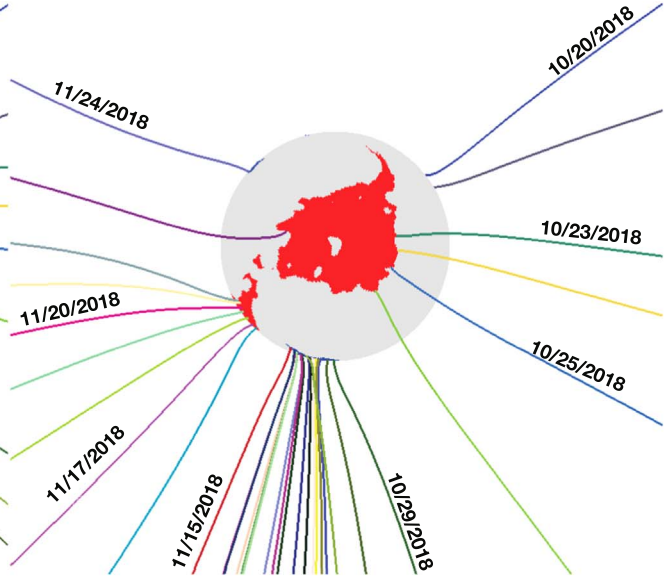
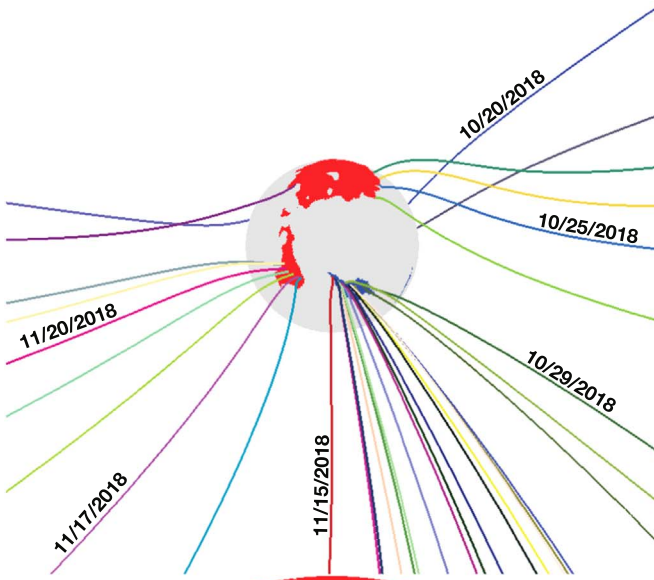
line. We note that during the week prior to first encounter, the field lines all traced back to the positive-polarity northern polar coronal hole. Just prior to first encounter (2018 October 29), the connectivity to the spacecraft jumped to the negative-polarity equatorial coronal hole. *PSP* remained connected to this region for the entire first encounter, finally becoming connected with the positive-polarity, equatorial coronal hole on 2019 November 16. Several further points are worth noting. First, during first encounter, the field lines are bunched together (see panel (b), in particular). However, given the rapid acceleration of the spacecraft by this point, and the fact that it was reaching and exceeding corotation speeds, we cannot make any inferences on the expansion properties of the field lines. Second, during the central portion of the encounter, the field lines shown actually “wrap around” one another, indicating that the source region of plasma measured at *PSP* reversed toward the east, if only briefly. Again, this should be interpreted carefully: these are not field lines at a single point in time, but a sequence of field lines drawn on successive days. Third, initial connectivity with the equatorial hole is complex: on 2018 October 28, the field line connects to an eastward region of the CH, whereas one day later, it maps to the west-most portion of it.

We also computed a PFSS solution using the same combined (CR 2208+2209) synoptic map. The resulting coronal hole structure and the mapping of the field lines intercepting *PSP* are shown in Figure 3(d), and can be compared with the MHD results in panel (a). There are several similarities between the two solutions, although also some important distinctions. First, both solutions produce two equatorial coronal holes at roughly the same Carrington longitudes. Additionally, both solutions map to the same positive-polarity equatorial coronal hole for roughly the same intervals, spanning the first encounter. However, the size and shape of the equatorial holes are substantially different, with the PFSS solution producing much smaller areas, in spite of the fact that we set the source surface radius to $2.0 R_S$, which is typically lower than is usually used, and chosen to open coronal holes as much as possible. Moreover, prior to first encounter, the PFSS solution mapped to the negative-polarity southern polar coronal hole, and, thus, this transition would not be associated with a current sheet crossing.

By flying *PSP*’s trajectory through the heliospheric solution, we are able to recover the predicted plasma and magnetic field variables in situ. These are summarized in Figure 4. The panels

(a) MHD: Equatorial View

(b) MHD: North-Pole View



(c) MHD: Equatorial Close-up

(d) PFSS: Equatorial View

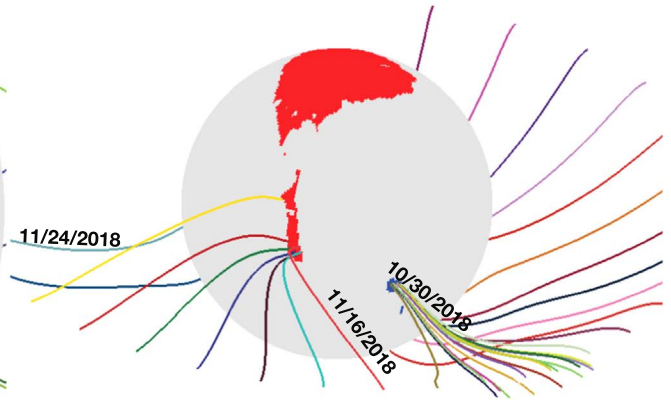
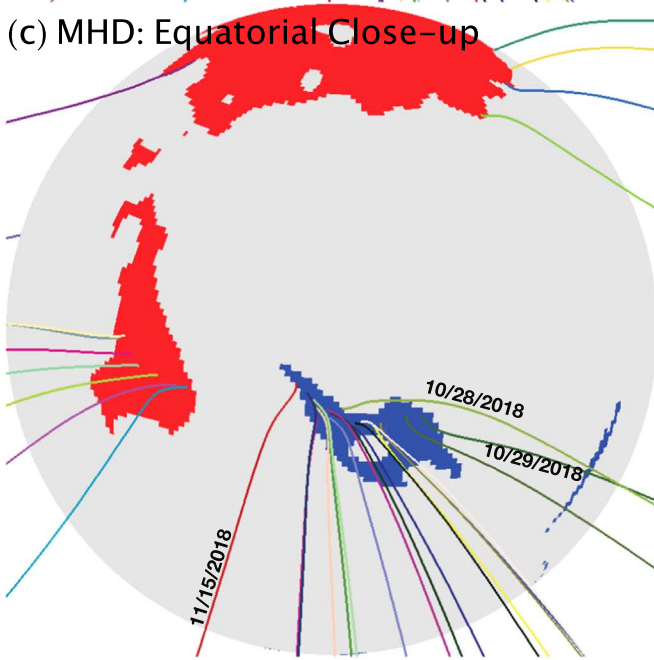


Figure 3. Mapping of field lines from *PSP*'s location in the inner heliosphere back to the solar surface. (a) Field lines (one per day) are shown mapped back to the coronal hole that they originated in using the MHD model solution. The underlying, observed polarity of the field is shown (red for radially outward field lines and blue for inward field lines). (b) The same field lines are shown from a view above the north pole of the Sun. (c) An equatorial close-up view of the same results. (d) Similar field lines are mapped back to the surface using a PFSS model solution, where the spacecraft location has been first ballistically mapped back to $2.0 R_S$.

show, from top to bottom, radial speed, radial component of the magnetic field (B_r), scaled B_r , plasma number density (N_p), scaled N_p , and the heliocentric position of the spacecraft, as summarized by distance (R) and Carrington longitude. Focusing first on panels (a), (b), and (d), we note the following points. First, the speed remained approximately constant during the interval from first encounter to second encounter ($\sim 525 \text{ km s}^{-1}$). Second, the magnetic field switched from positive polarity to negative polarity (day of year: 302), and remained so for approximately three weeks. It also increased to a maximum negative value of -80 nT . Third, plasma density rose to almost 80 cm^{-3} ; however, the peak in density lagged the magnetic field peak by approximately one day.

These variations, however, are misleading, in the sense that both the density and radial magnetic field fluctuations lie on top of the geometric expansion of the solar wind, which naturally produces a $1/r^2$ fall off with heliocentric distance, or, because the spacecraft is moving toward perihelion, an increase of r^2 . To address this, in panels (c) and (e) of Figure 4, we have removed the $1/r^2$ variation and scaled the measurements to 1 au values. Both the values and variations are markedly different (compare panels (b) and (c) and panels (d) and (e)). Now, B_r remains virtually flat ($\sim 8 \text{ nT}$) for the entire duration of the encounter. Number density, N_p , on the other hand, does have some intrinsic variations, peaking four days after perihelion (doy 314). This explains why the peaks in density

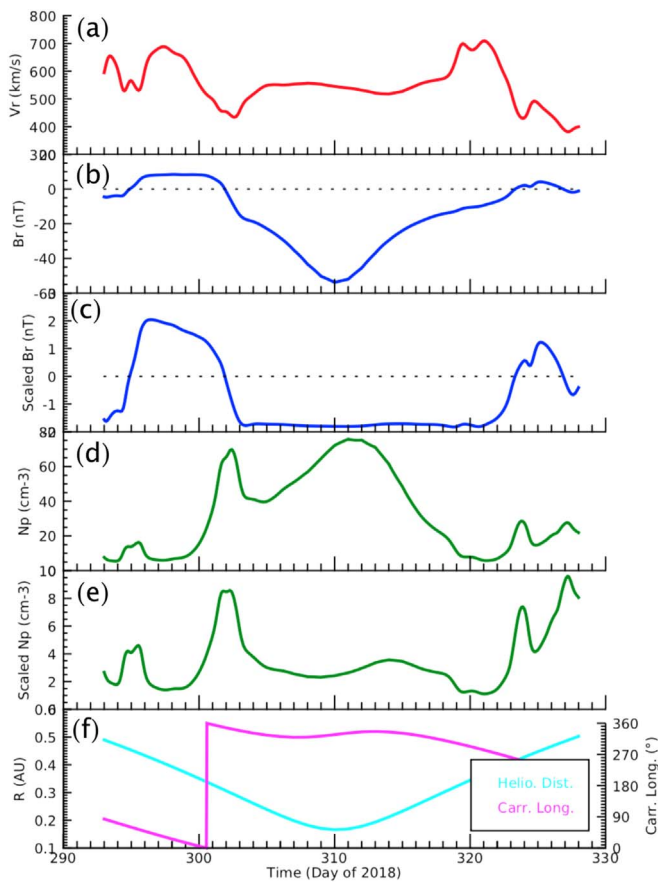


Figure 4. Time series of predicted (a) radial velocity (v_r), (b) radial magnetic field (B_r), (c) scaled B_r , (d) plasma number density (N_p), (e) scaled N_p , and (f) location of spacecraft in terms of heliocentric distance (aqua) and Carrington longitude (magenta). In (c) and (e), the radial magnetic field and number density have been scaled by r^2 to account for the radial fall-off expected from flow into a spherical geometry.

and magnetic field are not synchronous. The peak in field is due to the spacecraft reaching perihelion, i.e., it is an expansion effect, whereas the density is a superposition of this expansion effect with a later, intrinsic peak due to structure generated by the Sun.

5. Conclusions and Discussion

Based on the analysis presented here, we conclude that in the days prior to the first encounter *PSP* was connected to field lines originating in the well-established positive-polarity, northern polar coronal hole. During the encounter, and at perihelion in particular, field lines at the spacecraft mapped back to a negative equatorial coronal hole. After the encounter (beyond day 320), field lines were all connected to a positive-polarity, equatorial coronal hole to the east.

Our comparison of the magnetic mappings based on the MHD and PFSS solutions revealed some important differences. Although these differences have been discussed in the past, where it was shown that the MHD solutions generally yielded more accurate results (Riley et al. 2006), we cannot make that claim here; at least not yet. Until the magnetic field measurements (and, to a lesser extent, the plasma moments) have been sent back and fully analyzed, it is quite possible that the PFSS model is correct. It will be interesting to see whether the observations are consistent with a crossing of the current

sheet on day 302 (2018 October 29) as suggested by our MHD results, which was not predicted by the PFSS solutions.

It is interesting to compare our predictions with those of van der Holst et al. (2019). They also predicted a crossing of the HCS; however, in their model, this occurred at two points, 2018 November 3 and 2019 November 8, with the interval between them (and containing perihelion) being of negative polarity. In contrast, our model only predicted one crossing, occurring on 2018 October 29. Additionally, at perihelion, they predicted lower plasma speeds (360 km s^{-1} compared to our prediction of 525 km s^{-1}), higher densities (500 cm^{-3} compared to 80 cm^{-3}), and smaller radial magnetic field strengths (28 nT compared to 80 nT). Once the measurements from *PSP* become available, understanding these differences could be a crucial step for improving the accuracy of these models.

The model implemented here relied on a number of assumptions and approximations that might impact the accuracy of the results presented here. First, although the model used is time-dependent, in the sense of solving the time-dependent equations of MHD, the boundary does not evolve in time, thus, the solutions are “quasi-stationary.” Second, these boundary conditions are constructed from Earth-based observations of the photospheric magnetic field. Since *PSP* was approximately 90° to the west of Earth at the time of perihelion, the magnetic field lying underneath it at that time had been observed approximately seven days earlier (and shifted to the appropriate longitude in the Carrington map). Thus, the data used to derive the prediction at perihelion was approximately one week old. During this time photospheric fields can evolve significantly, as suggested by comparisons between CRs 2208, 2209, and 2210.

The analysis presented here highlights the value that global MHD models can contribute to missions like *PSP*. In particular, they provide a global context for interpreting in situ measurements made by the FIELDS and SWEAP instruments. Moreover, they can be used to support or refute theories of coronal heating and/or acceleration of the solar wind. Finally, they can be used to connect solar source regions to the structures and events measured in situ by the spacecraft. This will be particularly useful during observations of energetic particles (e.g., Schwadron et al. 2015).

The authors gratefully acknowledge support from NASA (80NSSC18K0100, NNX16AG86G, 80NSSC18K1129, and 80NSSC18K0101), NOAA (NA18NWS4680081), and the U.S. Air Force (FA9550-15-C-0001).

ORCID iDs

Pete Riley <https://orcid.org/0000-0002-1859-456X>
 Cooper Downs <https://orcid.org/0000-0003-1759-4354>
 Jon A. Linker <https://orcid.org/0000-0003-1662-3328>
 Zoran Mikic <https://orcid.org/0000-0002-3164-930X>
 Roberto Lionello <https://orcid.org/0000-0001-9231-045X>
 Ronald M. Caplan <https://orcid.org/0000-0002-2633-4290>

References

- Aschwanden, M. J., Burlaga, L. F., Kaiser, M. L., et al. 2008, *SSRv*, 136, 565
 Bale, S., Goetz, K., Harvey, P., et al. 2016, *SSRv*, 204, 49
 Caplan, R. M., Mikić, Z., Linker, J. A., & Lionello, R. 2017, *JPhCS*, 837, 012016
 Downs, C., Lionello, R., Mikić, Z., Linker, J. A., & Velli, M. 2016, *ApJ*, 832, 180

- Fox, N., Velli, M., Bale, S., et al. 2016, [SSRv](#), 204, 7
- Kasper, J. C., Abiad, R., Austin, G., et al. 2016, [SSRv](#), 204, 131
- Linker, J. A., Mikić, Z., Bisecker, D. A., et al. 1999, [JGR](#), 104, 9809
- Lionello, R., Downs, C., Linker, J. A., et al. 2013, [ApJ](#), 777, 76
- Lionello, R., Linker, J. A., & Mikić, Z. 2001, [ApJ](#), 546, 542
- Lionello, R., Velli, M., Downs, C., et al. 2014, [ApJ](#), 784, 120
- McComas, D., Alexander, N., Angold, N., et al. 2016, [SSRv](#), 204, 187
- Mikić, Z., & Linker, J. A. 1994, [ApJ](#), 430, 898
- Mikić, Z., Lionello, R., Downs, C., et al. 2018, in *Solar Wind 15*, ed. G. Lapenta (Brussels: AIP)
- Parker, E. N. 1958, [ApJ](#), 128, 664
- Pizzo, V. J., & Gosling, J. T. 1994, [GeoRL](#), 21, 2063
- Riley, P., Linker, J. A., & Mikić, Z. 2001, [JGR](#), 106, 15889
- Riley, P., Linker, J. A., Mikić, Z., et al. 2006, [ApJ](#), 653, 1510
- Riley, P., Lionello, R., Linker, J. A., et al. 2012, [SoPh](#), 274, 361
- Schwadron, N. A., Lee, M. A., Gorby, M., et al. 2015, [ApJ](#), 810, 97
- Török, T., Downs, C., Linker, J. A., et al. 2018, [ApJ](#), 856, 75
- van der Holst, B., Manchester, W. B., IV, Klein, K. G., & Kasper, J. C. 2019, [ApJL](#), 872, L18
- Verdini, A., & Velli, M. 2007, [ApJ](#), 662, 669
- Vourlidas, A., Howard, R. A., Plunkett, S. P., et al. 2016, [SSRv](#), 204, 83
- Zank, G. P., Matthaeus, W. H., & Smith, C. W. 1996, [JGR](#), 101, 17093